MicroRNA-124 loaded nanoparticles enhance brain repair in Parkinson's disease

C. Saraiva[a], J. Paiva[b,c], T. Santos[a], L. Ferreira[b,c,d] and L. Bernardino[a*]

[a]Health Sciences Research Centre, Faculty of Health Sciences, University of Beira Interior, 6201-506 Covilhã, Portugal; [b]CNC-Center for Neuroscience and Cell Biology, 3004-504 Coimbra, Portugal; [c]Biocant - Center of Innovation in Biotechnology, 3060-197 Cantanhede, Portugal; [d]Institute for Interdisciplinary Research, University of Coimbra (IIIUC), 3030-789 Coimbra, Portugal.

Corresponding Author
* libernardino@fcsaude.ubi.pt

Abstract

Modulation of the subventricular zone (SVZ) neurogenic niche can enhance brain repair in several disorders including Parkinson's disease (PD). Herein, we used biocompatible and traceable polymeric nanoparticles (NPs) containing perfluoro-1,5-crown ether (PFCE) and coated with protamine sulfate to complex microRNA-124 (miR-124), a neuronal fate determinant. The ability of NPs to efficiently deliver miR-124 and prompt SVZ neurogenesis and brain repair in PD was evaluated. *In vitro*, miR-124 NPs were efficiently internalized by neural stem/progenitors cells and neuroblasts and promoted their neuronal commitment and maturation. The expression of Sox9 and Jagged1, two miR-124 targets and stemness-related genes, were also decreased upon miR-124 NP treatment. *In vivo*, the intracerebral administration of miR-124 NPs increased the number of migrating neuroblasts that reached the granule cell layer of the olfactory bulb, both in healthy and in a 6-hydroxydopamine (6-OHDA) mouse model for PD. MiR-124 NPs were also able to induce migration of neurons into the lesioned striatum of 6-OHDA-treated mice. Most importantly, miR-124 NPs proved to ameliorate motor symptoms of 6-OHDA mice, monitored by the apomorphine-induced rotation test. Altogether, we provide clear evidences to support the use of miR-124 NPs as a new therapeutic approach to boost endogenous brain repair mechanisms in a setting of neurodegeneration.

Keywords: neural stem cells, miR-124, nanoparticles, neurogenesis, Parkinson's disease.

Introduction

Neurogenesis occurs constitutively in the subventricular zone (SVZ) of the adult mammalian brain, including in humans [1]. Within this region, neural stem cells (NSCs) can self-renew, proliferate and give rise to new neurons, astrocytes and oligodendrocytes. In rodents, newborn neurons generated in the SVZ migrate through the rostral migratory stream (RMS) towards the olfactory bulb (OB) where they fully differentiate as mature interneurons [2]. Adult neurogenesis homeostasis is altered in several brain disorders including Parkinson's disease (PD) [3]. PD is characterized by the loss of dopaminergic (DA) neurons present in the *substantia nigra* (SN) and degeneration of DA terminals in the striatum, leading to movement coordination impairments and cognitive deficits. Several factors have already been reported to improve functional recovery in PD animals models by increasing endogenous neurogenesis and migration of newly born neurons into the lesioned striatum [4,5]. However, an efficient therapy aiming at full regeneration has not yet been found. Therefore, it is imperative to find new platforms to efficiently deliver pro-neurogenic factors to NSCs and to boost the endogenous regenerative capacity of adult brain.

A tightly controlled network of intrinsic and extrinsic signals, including small non-coding RNAs (e.g. microRNAs) [6–9] regulate the neurogenic niche. MicroRNAs (miR) are able to regulate hundreds of genes [10] at the post-transcriptional level by inhibiting mRNA translation or inducing mRNA degradation [11]. MiR-124 is one of the most abundant miR in the adult brain [12]. The expression of miR-124 is initiated during the transition from NSC to progenitor cell and it is enhanced with neuronal maturation [13,14]. Several studies have shown that the overexpression of miR-124 induces neuronal differentiation of both progenitor cells [15,16] and HeLa cells [10]. More recently, lentiviral overexpression of the miR-124 precursor (among other factors) was capable of inducing the differentiation of human neonatal foreskin fibroblasts into functional mature neurons [17,18]. *In vivo*, miR-124 overexpression in the SVZ niche increased the number of newborn neurons without affecting their migratory capability [13,14]. Additionally, miR-124 is intimately associated with brain pathologies and neurodegenerative disorders, such as PD. Indeed, within the miR-124 validated targets, one-fourth are de-

regulated in PD (49 genes out of 202, MIRECORDS database) [19]. Significant decrease of miR-124 was described in the SN of 1-methyl-4-phenyl-1,2,3,6-tetrahydropyridine (MPTP)-intoxicated mice (PD mouse model) as well as in MN9D dopaminergic neurons treated with methyl phenyl pyridinium (MPP) iodide, while its overexpression improved cell survival [20,21]. Therefore, increasing miR-124 intracellular levels likely stands for a novel therapeutic strategy to improve functional outcome in PD (reviewed by Sun et al 2015 [3]). Due to the short half-life and poor stability of miR, their efficient delivery into cells in a safe and controlled way remains a challenge [22]. Viral vectors have a high capacity to deliver miR, however safety issues such as immunogenicity and the risk of triggering oncogenic transformation limits its translation potential [23]. Non-viral vectors such as polymeric nanoparticles (NPs), which avoid these safety issues, have been used by us and others to efficiently deliver proneurogenic molecules, including miR, into cells [7,23–25]. As so, we hypothesized that the use of polymeric NPs to deliver miR-124 could promote neurogenesis of SVZ NSCs both *in vitro* and *in vivo* and ultimately promote brain repair. To confirm this hypothesis we used a NP formulation formed by poly(lactic acid-*co*-glycolic acid) (PLGA) and perfluoro-1,5-crown ether (PFCE), a fluorine compound that can be tracked non-invasively by ^{19}F-MRI, and coated with protamine sulfate to complex miR-124 [26]. The neurogenic potential of this NP formulation was assessed both in physiologic conditions and in a 6-hydroxydopamine (6-OHDA) mouse model for PD. We have found that miR-124-loaded NPs (miR-124 NPs) enhanced neuronal differentiation and axonogenesis *in vitro*. Accordingly, mRNA and protein levels of both Sox9 and Jagged1, two key non-neuronal genes, were also decreased upon miR-124 NP treatment. *In vivo*, a single administration of miR-124 NPs into the lateral ventricles of both healthy and 6-OHDA-lesioned mice was able to significantly increase the number of migrating neuroblasts that reached the granule cell layer of the OB. Importantly, miR-124 NPs also potentiated the migration of SVZ-derived new neurons towards the 6-OHDA lesioned striatum and decreased the motor impairments found in 6-OHDA treated mice. Altogether, our results support the therapeutic potential of miR-124 NPs as an enhancer of endogenous brain repair mechanisms.

Materials and Methods

Preparation of PLGA NPs.

PLGA NPs were prepared as described by Gomes and colleagues [26]. Briefly, PLGA (Resomers 502 H; 50:50 lactic acid/glycolic acid) (Boehringer Ingelheim Lda, Ingelheim, Germany) was covalently conjugated to fluoresceinamine (Sigma-Aldrich Co. LLC). NPs were prepared by dissolving PLGA (100 mg,) in a solution of dichloromethane/trifluoro-ethanol (1:8) containing PFCE (100 mg) (Fluorochem, Derbyshire, UK). This solution was then added dropwise to a poly(vinyl alcohol) (PVA) solution (5% w/v in water) and stirred. NPs were centrifuged and washed with distilled water before freeze-drying. NPs were coated with protamine sulfate (PS) in 1:1 ratio by agitation at room temperature (RT). After this incubation period, NPs were dialyzed (MWCO of 50 kDa) against distilled water, frozen and lyophilized to obtain a dry powder that was stored in a desiccator at RT.

Complexation of NPs with miR and cell transfection.

NPs were weighed and sterilized under ultraviolet light before being resuspended in SVZ cell culture medium devoid of growth factors and sonicated (Transsonic T460/HH, Elma Schmidbauer GmbH, Singen, Germany). To this suspension (1 to 20 µg/mL final concentration, specified in the text) a total of 200 nM of miR (miR-124 or scramble-miR, both from GE Healthcare Dharmacon Inc., Chicago, USA) were added and allowed to complex for 45 min at 37 ºC with intermittent agitation (Figure 1A). Void NPs were prepared using the same procedure but without adding miR. Cells were then incubated with void or miR-loaded NPs for 4 h at 37 ºC in an incubator with 5% CO_2 and 95% atmospheric air. All miR are from GE Healthcare Dharmacon Inc. and were provided annealed, desalted and in the 2'-hydroxyl form and were resuspended in sterile RNA free water. MiR-124 mature sequence is 5'UAAGGCACGCGGUGAAUGCC3'.

Characterization of NPs.

Particle size and zeta potential of NP suspensions were determined using light scattering *via* a Zeta PALS zeta potential analyzer and ZetaPlus Particle Sizing Software (Brookhaven Instruments Corporation, NY, USA). Size measurements were performed at 25 ºC, and data were recorded at a 90º angle, with an equilibration time of 2.5 min

and individual run times of 60 s. The average diameters described are number-weighted average diameters. The zeta potential of NPs was determined in aqueous solutions, at 25 ºC.

SVZ cell cultures and experimental treatments.

SVZ cell cultures were prepared from 1 to 3 day-old C57BL/6 mice as described by us [27]. Briefly, brains were removed and placed into HBSS solution supplemented with 100 U/mL penicillin and 100 µg/mL streptomycin (all from Life Technologies, Carlsbad, CA, USA). SVZ fragments were dissected from 450 µm-thick coronal brain sections and digested in 0.025% trypsin, 0.265 mM EDTA (all from Life Technologies), followed by mechanical dissociation. The single cell suspension was diluted in serum-free medium (SFM) composed of Dulbecco's modified Eagle medium [(DMEM)/F12 + GlutaMAX™-l)] supplemented with 100 U/mL penicillin, 100 µg/mL streptomycin, 1% B27 supplement, 10 ng/mL epidermal growth factor (EGF), and 5 ng/mL basic fibroblast growth factor-2 (FGF)-2 (all from Life Technologies) and plated onto uncoated petri dishes (Corning Life Science, NY, USA) and allowed to develop in an incubator with 5% CO_2 and 95% atmospheric air at 37 ºC. In these conditions, SVZ cells grow in suspension and generate neurospheres that are rich in neural and progenitor stem cells at distinct stages of differentiation and with proliferative and self-renewing abilities, as previously shown by us [7,24,27–30]. Five to six-day-old neurospheres were seeded onto 0.1 mg/mL poly-D-lysine- (PDL; Sigma-Aldrich Co. LLC, St. Louis, MO, U.S.A.) coated glass coverslips, or in PDL-coated 6-well plates for quantitative (q)PCR analysis and in 24-well plates for all the remaining experiments, in SFM medium devoid of growth factors. Two days after, medium was renewed and the cell monolayer was allowed to develop for different time frames in the presence of void, scramble-miR or miR-124 NPs.

Internalization studies.

SVZ cells were transfected with 10 µg/mL of fluorescein-labeled NPs (FITC-NPs) complexed with 400 nM of miR-Dy547 (GE Healthcare Dharmacon Inc.) for 4 h at 37 ºC, rinsed and maintained in SFM medium devoid of growth factors for 24 h. Thereafter cells were fixed with 4% paraformaldehyde (PFA), permeabilized and blocked with 6% bovine serum albumin (BSA; Amresco LLC, Solon, USA) and 0.5% Triton X-100

(Fisher Scientific, Pittsburgh, PA, USA) in 0.1 M of phosphate buffered-saline (PBS) for 1 h at RT. SVZ cells were then incubated overnight (ON) with the following primary antibodies: mouse monoclonal anti-nestin (1:100, Abcam Plc., Cambridge, UK), rabbit polyclonal anti-GFAP (1:200, Abcam Plc.), goat polyclonal anti-FITC (1:200, Abcam Plc.), goat polyclonal anti-DCX (1:200, Santa Cruz Biotechnology, Inc., Dallas, TX, U.S.A.) and mouse monoclonal anti-FITC (1:100, Sigma-Aldrich Co. LLC), all prepared in 0.3% BSA and 0.1% Triton X-100 solution. The secondary antibodies used were the following: Alexa Fluor 647 donkey anti-mouse, Alexa Fluor 350 goat anti-rabbit, Alexa Fluor 488 donkey anti-goat or mouse and Alexa Fluor 647 donkey anti-goat (all 1:200, Life Technologies). Whenever appropriated, nuclei were stained with Hoechst-33342 (4 µg/mL in PBS, Life Technologies) for 5 min at RT. After, cells were mounted in Fluoroshield Mounting Medium (Abcam Plc.) and photomicrographs taken using a confocal microscope (AxioObserver LSM 710, Carl Zeiss, Jena, Germany).

PI incorporation.

SVZ cells were treated with NPs and maintained in culture for 48 h after transfection. Propidium iodide (PI; 5 µg/mL; Sigma-Aldrich Co. LLC) was added in the last 10 min of the experimental protocol. Subsequently, cells were fixed with 4% PFA for 10 min, stained with Hoechst-33342 (4 µg/mL, Life Technologies) for 5 min at RT and mounted in Fluoroshield Mounting Medium (Abcam Plc.). Photomicrographs of PI incorporation were taken using an AxioImager microscope (Carl Zeiss, Göttingen, Germany).

TUNEL assay.

SVZ cells were fixed with 4% PFA and permeabilized in 0.25% Triton X-100 for 30 min at RT. After permeabilization cells were incubated for 10 min with 3% H_2O_2. Cells were then allowed to react for terminal transferase (0.25 U/L) biotinylated dUTP (6 M) nick-end labeling of fragmented DNA in TdT buffer (pH 7.5) (all from Roche, Basel, Switzerland) for 1 h at 37 ºC in a humidified chamber. The enzymatic reaction was stopped by rinsing with PBS. Cells were then incubated for 1 h with rhodamine (1:200, Vector Laboratories, Burlingame, CA, USA), rinsed and stained with Hoechst-33342 (4 µg/mL in PBS; Life Technologies) as described previously. Then, cells were mounted

in Fluoroshield Mounting Medium (Abcam Plc.). Photomicrographs were obtained using an AxioImager microscope (Carl Zeiss).

BrdU incorporation.

5-bromo-2'-deoxyuridine (BrdU; 10µM, Sigma-Aldrich Co. LLC) was added to cultures 4 h before the end of the experiment. Thereafter, cells were fixed in 4% PFA and BrdU was exposed following permeabilization with 1% Triton X-100 for 30 min at RT and an incubation with 1 M HCL for 40 min at 37 ºC. Nonspecific binding sites were blocked with 6% BSA and 0.3% Triton X-100 for 1 h, followed by incubation with anti-BrdU Alexa-Fluor 594 conjugated antibody (Life Technologies) prepared in 0.3% BSA and 0.3% Triton X-100 for 2 h at RT. Cells where then stained with Hoechst-33342 and mounted in Fluoroshield Mounting Medium (Abcam Plc.). Photomicrographs of BrdU incorporation were taken using a confocal microscope (AxioObserver LSM 710, Carl Zeiss).

Immunocytochemistry.

SVZ cultures were fixed with 4% PFA, permeabilized and blocked for non-specific binding sites for 1 h with 0.25% Triton X-100 and 3% BSA (cytoplasmatic staining) or 6% BSA (nuclear staining). Cells were subsequently incubated ON at 4 ºC with primary antibody. Cells were then incubated for 1 h with the corresponding secondary antibody followed by Hoechst-33342 nuclear staining, and mounted in Fluoroshield Mounting Medium (Abcam Plc.). Primary antibodies used were: rabbit polyclonal anti-ki67 (1:50, Abcam Plc.); mouse monoclonal anti-GFAP (1:200, Abcam Plc.); goat polyclonal anti-DCX (1:200, Santa Cruz Biotechnology, Inc.); mouse monoclonal anti-NeuN (1:100, Merck Millipore, Darmstadt, Germany); rabbit polyclonal anti-Olig2 (1:200, Merck Millipore); rabbit polyclonal Phospho-JNK (1:100, Cell Signaling, Beverly, MA, USA); mouse polyclonal anti-Tau (1:200, Cell Signaling); rabbit polyclonal anti-sox9 (1:200, Merck Millipore); goat polyclonal anti-jagged1 (1:100, Santa Cruz Biotechnology, Inc.), all prepared in 0.3% BSA and 0.1% Triton X-100. Secondary antibodies used were: Alexa Fluor 546 donkey anti-rabbit or mouse or goat and Alexa Fluor 488 donkey anti-mouse or rabbit (all 1:200, Life Technologies). Photomicrographs were taken using an AxioImager microscope or AxioObserver LSM 710 confocal microscope (both from Carl Zeiss).

Quantitative PCR (qPCR) analysis.

Total RNA was isolated from SVZ cell cultures according to the illustra RNAspin mini RNA isolation kit manufacturer's instructions (GE Healthcare Life Sciences, Cleveland, OH, USA). cDNA was prepared from 1 µg total RNA using the iScript cDNA synthesis kit (Bio-Rad Laboratories, Inc., Hercules, CA, USA). Briefly, 1 µg of RNA was mixed with 4 µL of 5x reaction mix and 1 µL of reverse transcriptase followed by the reaction in a T100 thermal cycler (Bio-Rad Laboratories, Inc.): 5 min at 25 ºC, 30 min at 42 ºC and 5 min at 85 ºC. qPCR was performed by adding 0.5µL of sample cDNA to 5µL SYBR Green PCR master mix (Bio-Rad Laboratories, Inc.) and 1 µL of GAPDH, Sox9 or Jag1 primers (all Qiagen, Austin, TX, USA) in a total volume of 10 µL. The thermocycling reaction was performed in a CFX Connect real-time system (Bio-Rad Laboratories, Inc.): 3 min at 94 ºC followed by 40 cycles of 15 s at 94 ºC denaturation step, 30 s at 60 ºC annealing and elongation step. Quantification of target genes was performed relative to the reference gene GAPDH using the comparative Ct method, as previously reported by us [7,25].

In vivo studies.

All animal experimental procedures were performed in accordance with institutional animal house, national and European Community guidelines (86/609/EEC; 2010/63/EU). Adult male C57BL/6 mice (Harlan Laboratories Models, SL, Castellar, Spain) with 10-12 week-old were used. All mice were housed in the same room and in similar cages under controlled conditions: 12 h light/dark cycle in room temperature (22 ºC) and *ad libitum* access to food and water.

Stereotaxic injections and BrdU administration.

Mice were anesthetized with an intraperitoneal (i.p.) injection of ketamine (90 mg/kg of mouse weight; Imalgene 1000, Merial, Lyon, France) and xylazine (10 mg/kg of mouse weight; Rompun 2%, Bayer, Leverkusen, Germany) before placing them in the digital stereotaxic frame (51900 Stoelting, Dublin, Ireland). An incision was performed with a scalpel to expose the mouse skull and scales were defined after setting the zero at the bregma point. An intraventricular injection of 2.5 µL of miR-124 NPs (1 µg/mL of NPs

loaded with 200 nM miR-124) or saline solution (0.9% NaCl) was performed in the right hemisphere (Anterior-posterior: −0.5 mm, Medial-lateral: −0.7 mm, Dorsoventral: −2.9 mm) [8] using a Hamilton syringe at a speed of 0.5 µL/min. To unveil the effect of our NP formulation in a mouse model for PD, mice were subjected to a double stereotaxic injection to deliver the 6-OHDA toxin into the right striatum and the NPs into the right lateral ventricle, as described previously. A total of 10 µg of 6-OHDA (Sigma-Aldrich Co. LLC) dissolved in 0.02% of ascorbic acid (Fagron, Inc., St. Paul, MN, USA) was injected *per* animal in the right striatum (Anterior-posterior: −0.6 mm, Medial-lateral: −2.0 mm, Dorsoventral: −3.0 mm) [31] with a Hamilton syringe at a speed of 0.2 µL/min. After injections, mice were kept warm (37 ºC) until they recovered from surgery. Four experimental groups were tested: 1) mice injected with saline both in the striatum and in the lateral ventricle – "Healthy Saline"; 2) mice injected with saline in the striatum and miR-124 NPs in the lateral ventricle- "Healthy miR-124 NP"; 3) mice injected with 6-OHDA in the striatum and saline in the lateral ventricle- "6-OHDA Saline"; 4) mice injected with 6-OHDA in the striatum and miR-124 NPs in the lateral ventricle- "6-OHDA miR-124 NP". To label dividing cells, BrdU dissolved in a sterile solution of 0.9% NaCl was administered i.p. (50 mg/kg of animal weight) in the following three days (every 12 h) after the stereotaxic procedure (Figure 7A). Mice were maintained in controlled conditions during the four weeks of experimental procedure before being euthanized. For internalization studies 3 µL of 10µg/mL of FITC-NPs complexed with 400nM of miR-Dy547 (dissolved in saline solution) were injected into the lateral ventricle of mice as described above and 24 h after injection the mice were euthanized.

Apomorphine-induced rotation test.

At week 2 post-stereotaxic injections, the mice received in the neck a subcutaneous injection of 0.5mg/kg of apomorphine hydrochloride (Sigma) dissolved in 1% ascorbic acid and 0.9% NaCl. Mice were placed in round testing bowls for 45 min and their behavior was recorded using a digital camera. Number of net contralateral turns = contralateral turns – ipsilateral turns; data are presented as percentage of 6-OHDA saline mice.

Immunohistochemistry.

Mice were deeply anesthetized with a mixture of ketamine and xylazine, and then perfused intracardially with saline solution followed by 4% PFA. Brains were surgically removed and post-fixed with 4% PFA for 24 h, followed by immersion in a 30% sucrose solution (Fisher Scientific) until sunk. Thereafter, brains were cryopreserved and 40 µm-thick coronal sections from the olfactory bulb (OB) or SVZ/striatum regions were collected in series of six slices (spaced 240 µm from each other), using a cryostat (CM 3050S, Leica Microsystems, Wetzlar, Germany). Immunostaining of tissue sections was performed by adapting the experimental protocol described elsewhere [32]. Briefly, tissue sections were rinsed in PBS and incubated with 2 M HCl for 25 min at 37 ºC to induce DNA denaturation and exposure of BrdU. Tissue sections were then incubated in blocking solution – 2% of horse serum (Life Technologies) and 0.3% Triton X-100 in PBS – for 2 h at RT, followed by a 48 h incubation at 4ºC with the following primary antibodies: rat monoclonal anti-BrdU (1:500, AbD Serotec, Raleigh, NC, U.S.A.), and goat polyclonal anti-DCX (1:1000, Santa Cruz Biotechnology, Inc.), or mouse monoclonal anti-NeuN (1:1000, Merck Millipore). Thereafter, sections were incubated for 2 h at RT with Hoechst (1:10,000) and the respective secondary antibodies: Alexa Fluor 488 donkey anti-rat, Alexa Fluor 546 donkey anti-goat or anti-mouse (all 1:1000; from Life Technologies). Then, a simplified version of this protocol was used for internalization studies. Briefly, 40 µm-thick coronal sections were incubated in blocking solution for 1 h at RT and then incubated for 48 h at 4ºC with the goat polyclonal anti-FITC (1:500, Abcam Plc.). Thereafter, sections were incubated for 2 h at RT with Hoechst (1:10,000) and the secondary antibody, Alexa Fluor 488 donkey anti-goat (1:1000, Life Technologies). Finally, sections were mounted in Fluoroshield Mounting Medium (Abcam Plc.). Photomicrographs were obtained using an AxioObserver LSM 710 confocal microscope (Carl Zeiss).

Statistical analysis.

Analysis of immunocytochemistry experiments were performed at the border of seeded neurospheres, where cells formed a pseudo-monolayer. The experiments were performed in three independent cultures, unless stated otherwise, and for each experimental condition at least 2 coverslips were assayed *per* culture. Percentage of fragmented nuclei, TUNEL[+], PI[+], BrdU[+], Ki67^{+}, Ki67^{+}/DCX[+], Ki67^{+}/GFAP[+], NeuN[+], GFAP[+], Olig2^{+}, Sox9^{+} and Jagged1^{+} was calculated from cell counts in five independent

microscopic fields (approximately 150 cells *per* field) from each coverslip with a 40x magnification. Quantification of neurite ramification number and total neurite length positive for P-JNK was performed in 4 independent cultures, with at least 2 coverslips *per* condition, in approximately 20 non-overlapping fields *per* coverslip (40x magnification).

Quantification of DCX$^+$, DCX$^+$/BrdU$^+$ and NeuN$^+$/BrdU$^+$ cell number was performed in the SVZ, OB (granule (GCL) and glomerular (GL) layers) and striatum of at least 3 animals, as described previously by us [8]. For the SVZ, 5 slices spaced by 240 µm each were used. Cells were counted along the ventricle lateral wall from three different Zaxis-positions *per* field in a 40x magnification (totaling approximately 35 fields *per* mouse hemisphere). To obtain an unbiased density estimate, fields with the same mean total volume and total number of SVZ cells were selected. In the OB, two fields of GCL and six fields of GL from three different Zaxis-positions *per* field from 4 slices spaced by 240 µm each were counted *per* animal. In the striatum, two different Zaxis-positions from nine fields from 5 slices spaced by 240 µm each were counted *per* animal.

The software used for cell countings was ImageJ (NIH Image, Bethesda, MD, USA). Data were expressed as mean ± standard error of mean (SEM). Statistical significance was determined with GraphPad Prism 6 software (GraphPad, San Diego, CA, USA) by using ANOVA followed by Dunnett's or Bonferroni's test or unpaired two tailed Student's t test, with $p < 0.05$ considered to represent statistical significance.


Results and Discussion

miR-loaded NPs are efficiently internalized by SVZ cells.
Novel polymeric PLGA-based NPs developed by us were used to deliver miR-124 into SVZ cells (Figure 1A). These NPs have an average size of ~210 nm and are coated with protamine sulfate, a cationic peptide that confers a positive surface charge (+5.7 ± 1.2 mV, n=3) to the NP, allowing their complexation with miR (negatively charged molecule) (+1.7 ±0.7 mV, n=3). Moreover, NPs have in its core PFCE, a nontoxic fluorine compound commonly used in nuclear magnetic resonance (NMR) imaging applications, allowing *in vivo* non-invasive tracking of NPs (Figure 1A) [26,33]. First, the ability of distinct SVZ cell phenotypes to internalize NPs was evaluated by confocal analysis. Primary SVZ

cell cultures contain a mixture of stem (type B cells) and progenitor cells (type C cells) able to proliferate and generate neurons and glial cells [34]. SVZ cells were treated with 10 µg/mL of FITC-labeled NPs complexed with Dy547-labeled miR mimic (a fluorescent scramble-miR) for 4 h, washed out to remove non-internalized NPs, and maintained in culture for additional 24 h. A fluorescence scramble-miR was used since it does not alter significantly the formulation characteristics, such as size, zeta potential, complexation, and it is easier to track. The intracellular uptake of miR NPs by neural stem/progenitor cells and neuroblats was evaluated by co-staining doublecortin (DCX), glial fibrillary acidic protein (GFAP) or nestin (Figure 1B, C, D). At this time point, primary SVZ cultures contain approximately 10-20% neurons, 15-20% astrocytes and 70-80% immature cells (nestin$^+$/GFAP$^-$) (data not shown). We have found that miR-Dy547 NPs were efficiently internalized by neuroblasts (DCX-positive (DCX$^+$); Figure 1B), type B cells (GFAP$^+$/nestin$^+$; Figure 1C, D), immature progenitor cells (nestin$^+$ cells; Figure 1C arrow), and by astrocytes (GFAP$^+$; Figure 1D arrowhead). The development of efficient and safer delivery systems for miR is a major concern, since naked miR delivery presents a poor uptake efficiency caused mainly by miR hydrophilic nature and negative charge [22,23]. Our NP formulation proved to be efficient in both delivery and protection of miR. In fact, we showed recently that the same NP formulation was able to rapidly release miR in human umbilical vein endothelial cells (HUVEC), with only 50% of miR-Dy547 co-localizing with FITC-NPs at 24 h post-transfection [26]. Moreover, the retention of about 30% of NPs or miR-Dy547 within the endolysossomal compartments was associated with the ability of the NP formulation to present miR to the RNA-induced silencing complex (RISC) machinery. This characteristic culminated in a higher biologic effect than the commercial transfection system SIPORT, either in normoxia or hypoxia conditions [26]. In SVZ cells, miR-Dy547 and FITC-NPs labeling was located preferentially in aggregates during the initial hours but at 24 h post-transfection it was found spread all over the cell cytoplasm including in the cellular processes of type B cells, immature progenitor cells and new neurons (Figure 1B-D). The huge heterogeneity in cell phenotypes and density found in SVZ cultures hamper an extensive tracking of miR-Dy547 FITC-NPs inside SVZ cells. Nevertheless, miR-Dy547 FITC-NPs were found internalized in all SVZ cell types analyzed

suggesting that this formulation represents an efficient miR delivery vector. Importantly, our formulation was efficiently internalized and able to deliver miR-124 into stem/progenitor and immature cells, the cell population that in response to increased levels of miR-124 may differentiate into mature neurons. In accordance, internalization in mature neurons was not analyzed due to its already high basal expression of miR-124 [13].
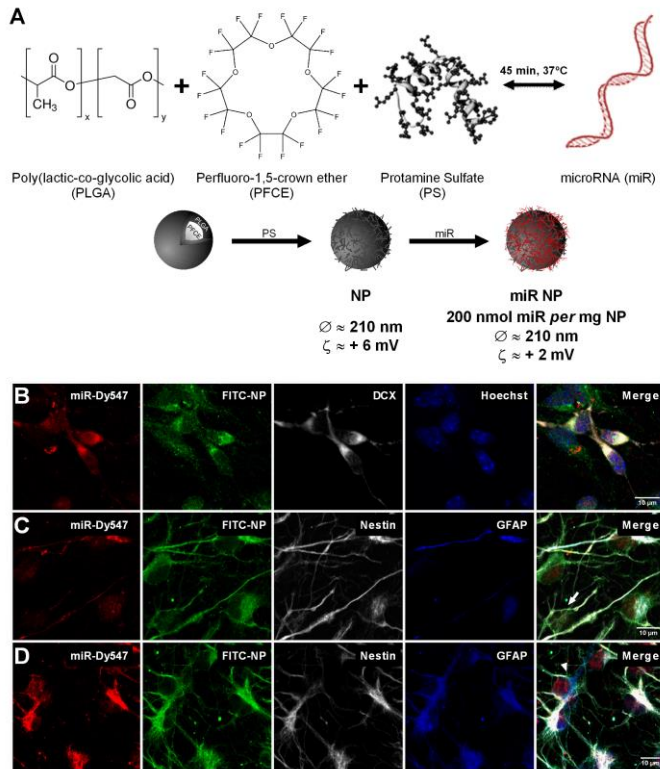
Figure 1. MiR loaded NPs are internalized by SVZ stem/progenitor cells. (A) Composition and physical properties of miR NPs. (B, C, D) Photomicrographs of SVZ stem/progenitor cells after transfection with 10 µg/mL of FITC-NPs (green) complexed with miR-Dy547 (red) and stained against immature neuronal marker DCX (white), and nuclear marker Hoechst (blue) (B) or the immature progenitor marker nestin (white) and the glial marker GFAP (blue) (C, D). FITC-NPs and miR-Dy547 were found internalized in all cell types analyzed. White arrow shows a cell that is only positive for nestin (immature cell) and arrowhead shows a cell exclusively positive for GFAP (astrocyte). Cells positive for both nestin and GFAP markers (type B cells) are also observed (C, D). Scale bar: 10 µm.

Cellular toxicity of NPs.

Next, the toxic effect of NPs on SVZ cells was assessed by nuclear condensation/fragmentation (Figure 2A), terminal deoxynucleotidyl transferase-mediated dUTP nick end labeling (TUNEL) (Figure 2B, D) and propidium iodide (PI) incorporation (Figure 2C, E) analysis. MiR-124 and void NPs at 1, 10 and 20 µg/mL were added to cells for 4 h. Thereafter, cells were rinsed to discard non-internalized NPs and maintained in culture medium for 48 h. A first screening in terms of cell toxicity was performed by quantifying the number of fragmented/condensed nuclei (labeled with Hoechst). Concentrations up to 1 µg/mL of void NPs and up to 10 µg/mL of miR-124 NPs did not induce significant nuclear condensation/fragmentation as compared with non-treated cells (Figure 2A). Scramble-miR NPs at 10 µg/mL were nontoxic as well (105.6 ± 13.6, n=3). Parameters such as composition, size, and superficial charge among other factors influence NP toxicity. NPs with higher surface charge generally present higher toxicity [35], which may explain the highest cytotoxicity of void (+5.7 ± 1.2 mV) *versus* miR NPs (+1.7 ±0.7 mV). Importantly, 1 µg/mL NPs either complexed or not with miR revealed no cytotoxicity. This concentration was then used to evaluate apoptosis and necrosis in SVZ cells treated with void NPs or miR NPs (scramble-miR or miR-124) by TUNEL and PI staining, respectively. We have found that 1 µg/mL NPs (void, scramble-miR or miR-124) did not induce apoptosis (Figure 2B, D) or necrosis/late-apoptosis (Figure 2C, E). Based on these results, 1 µg/mL NPs complexed with miR-124 was selected to perform the subsequent experiments.
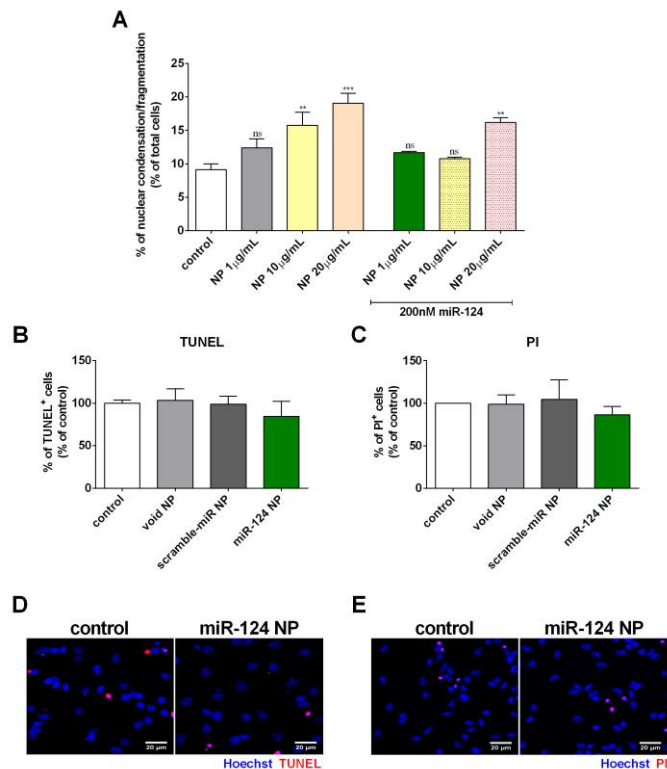
Figure 2. Viability studies in SVZ cells treated with NPs. SVZ stem/progenitor cells were treated for 4 h with NPs and then maintained in culture for 2 days. Percentage of (A) cells with nuclear condensation/fragmentation, (B) TUNEL+ apoptotic cells and (C) propidium iodide (PI)+ necrotic cells. Representative confocal digital images of (D) TUNEL, (E) PI, and Hoechst (blue) stainings in control cultures and in miR-124 NP treated cultures. Both TUNEL and PI stainings are shown in red. Scale bar: 20 µm. Data are expressed as mean ± SEM (n=3-13). **P < 0.01, ***P < 0.001 using Dunnett's multiple comparison test and compared with control. (B, C) Data are presented as percentage of control (set to 100%). ns, non-significant.

miR-124 NPs prompt neuroblasts proliferation

Next, we examined the effect of miR-124 NPs in cell proliferation by analyzing 5-bromo-2'-deoxyuridine (BrdU) and Ki67 staining 48 h after cell treatments. BrdU is a marker for cells undergoing S phase of the cell cycle, while all cycling cells (G1, S, G2 and M phases) express the Ki67 marker. Overall, total cell proliferation was not affected as compared with control cultures (Figure 3A, B). However, cells treated with miR-124 NPs showed a higher number of proliferating neuroblasts (Ki67+/DCX+; Figure 3C, E) and a lower number of proliferating astrocyte-like cells (Ki67+/GFAP+; Figure 3D, F) when compared with the respective controls. Thus, our results indicate that miR-124 NPs favor

neuroblast proliferation while decreasing the proliferation of astrocytic-like cells. In accordance, others have showed that viral overexpression of miR-124 is able to promote the commitment of type C progenitor cells towards a neuronal fate while reducing the stem/progenitor cell pool [13,14]. In physiological conditions, the expression of mir-124 is also increased during the transition from progenitors towards mature neuronal cells [13,14].
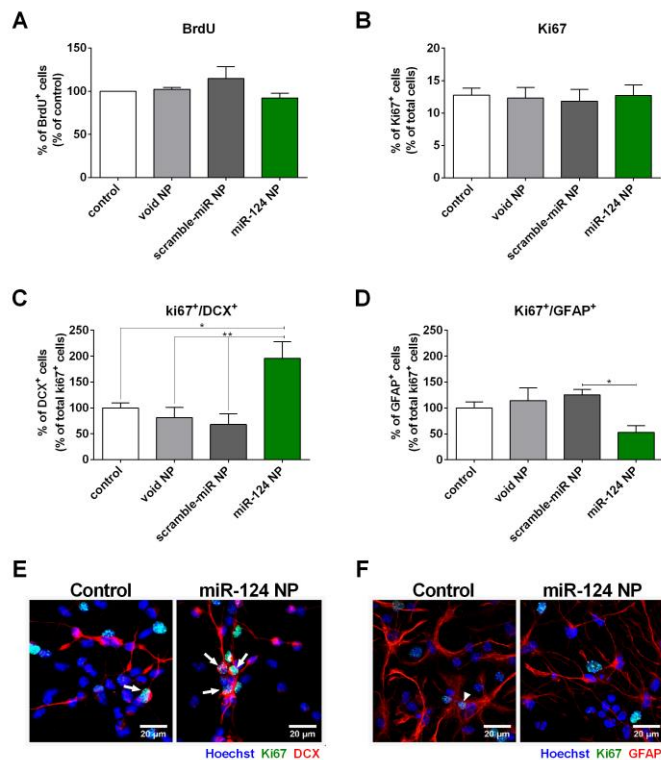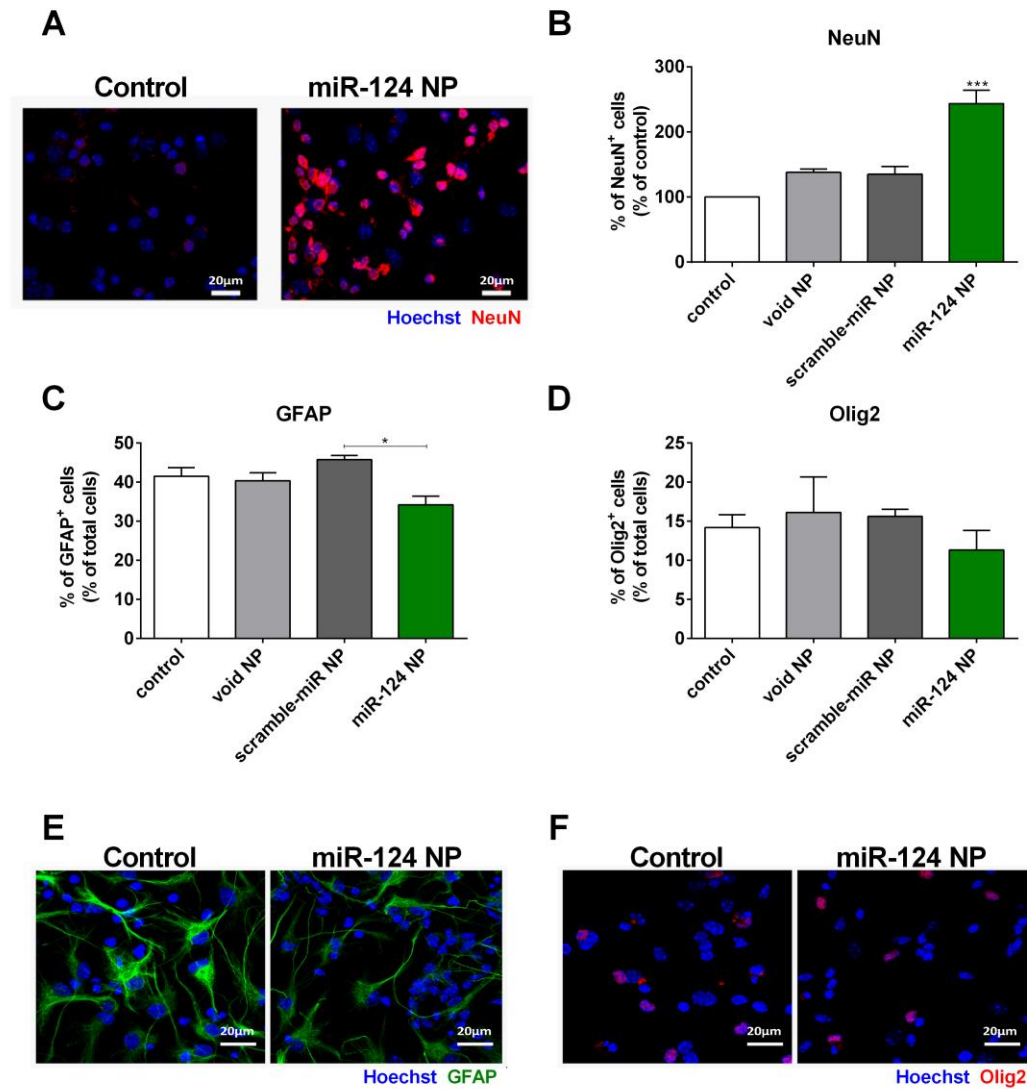

Figure 3. MiR-124 NPs favor neuroblast proliferation. SVZ stem/progenitor cells were treated for 4 h with NPs and then maintained in culture for 48 h. (A, B) Bar graphs depict the percentage of BrdU$^+$ and Ki67$^+$ cells, respectively. Percentage of (C) DCX$^+$ or (D) GFAP$^+$ cells co-labeled with Ki67 staining. Representative fluorescence photomicrographs of (E) DCX/Ki67 and (F) GFAP/Ki67 immunostainings in control cultures and in miR-124 NP treated cultures. Nuclei are shown in blue, Ki67 in green and, DCX and GFAP in red. Scale bar: 20 µm. White arrows depict double-positive cells. Data are expressed as mean ± SEM (n=2-3). *P < 0.05, **P < 0.01 using Bonferroni's multiple comparison test. (A, C, D) Data are presented as percentage of control (set to 100%).

miR-124 NPs induce neuronal differentiation by repressing key non-neuronal genes.

The ability of miR-124 NPs to induce neuronal differentiation was then assessed. As shown in Figure 4, miR-124 NPs led to a 2.5-fold increase in the number of mature neurons (NeuN; Figure 4A, B) while reducing to approximately 25% the number of astrocytes (GFAP; Figure 4C, E) as compared with scramble-miR NP-treated cells. No effects were found in terms of oligodendrocyte differentiation (oligodendrocytes transcription factor 2 (Olig2); Figure 4D, F). Although the oligodendrocytic lineage is dependent on Olig2 expression, a subpopulation of stem/progenitor cells also express Olig2 [36]. These data are in accordance with the results shown in Figure 3. Moreover, Akerblom and colleagues reported an increased number of astrocytes after miR-124 inhibition [14] and Neo and colleagues showed that miR-124 was able to control the choice between neuronal or astrocytic differentiation [37].

miR-124 targets include several non-neuronal-related genes including Sox9 (Notch downstream effector involved in glial fate specification and in the maintenance of stem cells in an undifferentiated state) [13,38,39] and jagged1 (Notch1 ligand involved in stem cell self-renewal) [13,38,40], among others. Therefore, the mRNA and protein levels of Sox9 and Jagged1 (Jag1) were evaluated by qPCR and immunocytochemistry, respectively. As expected, miR-124 NPs induced a reduction of approximately 30% in mRNA (Figure 5A) and a reduction of almost 50% in protein levels (Figure 5B, C, D, E) of both Sox9 and Jagged1. Altogether, our results indicate that miR-124 NPs modulate SVZ cells fate and downregulate Sox9 and Jagged1, leading to a robust enhancement of neurogenesis and a slight reduction in the number of astrocytes.

Figure 4. MiR-124 NPs promotes neuronal differentiation over glial differentiation. SVZ stem/progenitor cells were treated for 4 h with NPs and then maintained in culture for 7 days. (A) Representative fluorescence photomicrographs of NeuN immunostaining (red) in control cultures and cultures transfected with 1 µg/mL of miR-124 NPs. Hoechst was used for nuclear staining (blue); scale bar: 20 µm. (B) Percentage of NeuN-immunostained neurons, (C) GFAP-immunostained astrocytes and (D) Olig2-immunostained oligodendrocytes in SVZ cultures. Representative fluorescence photomicrographs of (E) GFAP (green) and (F) Olig2 (red) immunostainings in control cultures and in miR-124 NP treated cultures. Nuclei are shown in blue. Scale bar: 20 µm. Data are expressed as mean ± SEM (n=3-6). *P < 0.05, ***P < 0.001 using Bonferroni's multiple comparison test. In (B) data are presented as relative to control (set to 100%) and the statistics compares miR-124 NPs against all other experimental conditions (control, void and scramble NPs).
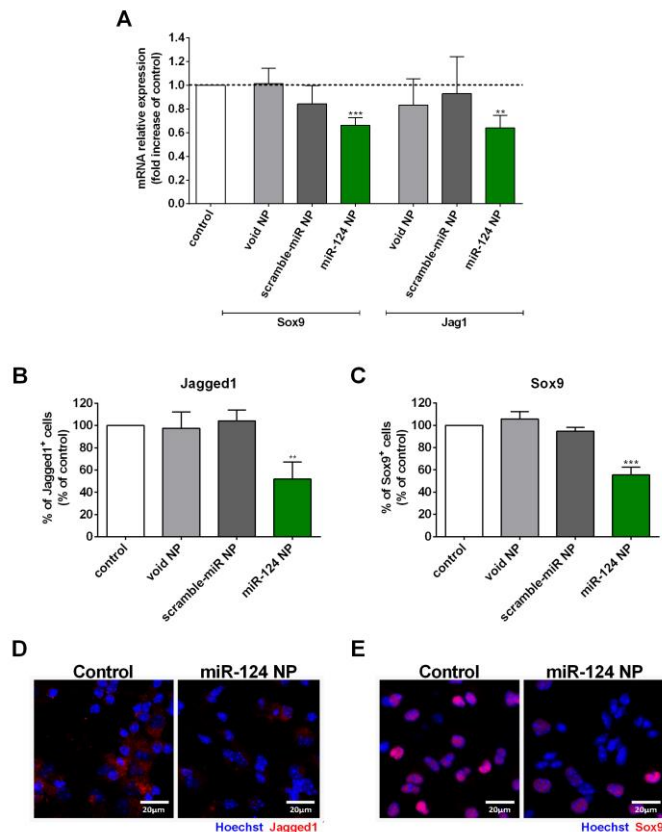
Figure 5. MiR-124 NPs target Sox9 and Jagged1 mRNA and protein levels. SVZ cells were treated for 4 h with NPs and maintained in culture for 5 or 7 days. (A) Sox9 and Jag1 mRNA expression 5 days after NPs treatment. Gene expression was normalized to GAPDH. Data are expressed as mean ± SEM (n=3-6). All data are presented as fold increase of control (set to 1). Percentage of (B) Jagged1$^+$ and (C) Sox9$^+$ cells in SVZ cultures 7 days after treatment with 1µg/mL miR-124 NPs. Representative fluorescence photomicrographs of (D) Jagged1 and (E) Sox9 immunostainings in control cultures and in miR-124 NP treated cultures. Nuclei are shown in blue. Scale bar: 20 µm. Data are expressed as mean ± SEM (n=3-6). **P < 0.01, ***P < 0.001 using Bonferroni's multiple comparison test and compared with control. (B, C) Data are presented as percentage of control (set to 100%).

miR-124 NPs promote axonogenesis.

Axon formation and neurite outgrowth are essential processes for the maturation and integration of newborn neurons; these processes are dependent on c-Jun N-terminal kinases (JNK) pathway activation [41]. To evaluate the effect of miR-124 NPs on neuronal maturation and axonogenesis, SVZ cells were transfected with miR-124 NPs for 4 h and the activation of SAPK/JNK pathway was analyzed 24 h post-transfection by immunocytochemistry against phospho (P)-JNK, the JNK active form. MiR-124 NPs

induced a 1.6 and 2-fold increase in the number (Figure 6A) and length (Figure 6B) of P-JNK⁺ axons emerging out of the neurospheres, respectively. Accordingly, in miR-124 NP-treated cultures P-JNK immunoreactivity was robust while control cultures showed a more diffuse and weak staining (Figure 6C). Also, as reported previously by us, the P-JNK staining co-localized with Tau, a microtubule-associated protein able to modulate the stability of axonal microtubules in mature and immature neurons [29,30].

JNK can phosphorylate and activate several transcription factors in the nucleus, including c-Jun, which may transduce cell death signals [42–44]. As shown in Figure 6C, P-JNK immunoreactivity was localized in Tau-positive axons, but not in the nucleus, suggesting that miR-124 NPs promote axonogenesis instead of inducing apoptosis. Additionally, neither apoptosis nor late-apoptosis/necrosis was induced by 1 µg/mL miR-124 NPs (Figure 2B, C, D, E). Indeed, growing literature supports a role of JNK in cell proliferation, survival, and differentiation. For instance, it was shown that JNK1 and the JNK pathway-specific scaffold protein, JSAP1, promote neural differentiation of embryonic stem cells [45,46]. Activated JNK may also foster axonogenesis and neuronal polarization by targeting cytoskeletal proteins, such as the Tau protein [47,48].

Our results are also in accordance with a previous report showing that miR-124 is able to control neurite outgrowth during neuronal differentiation presumably by regulating cytoskeleton proteins [15]. Additionally, it has been shown by others that miR-124 promotes neurite elongation in human neuroblastoma and mouse P19 cell lines by repressing Rho-associated coiled-coil forming protein kinase 1 (ROCK1), an upstream repressor of the phosphoinositide 3-kinase (PI3K)/Akt pathway [49]. In sum, the activation of the SAPK/JNK pathway found in Tau-expressing axons suggests that miR-124 NPs enhance axonogenesis and neuronal maturation in SVZ cells.
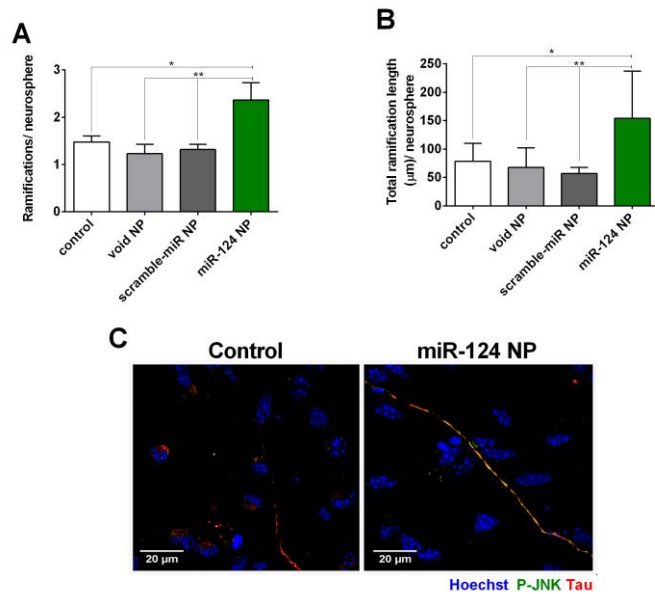
Figure 6. MiR-124 NPs activate the SAPK/JNK pathway in Tau$^+$ axons. SVZ stem/progenitor cells were treated for 4 h with NPs and then maintained in culture for 24 h. Bar graphs display (A) number of ramifications and (B) the total ramification length (µm) of P-JNK$^+$ fibers per neurosphere. (C) Representative fluorescence photomicrographs of P-SAPK/JNK (green), Tau (red), and Hoechst (blue) staining in control cultures and in miR-124 NP treated cultures; scale bar: 20 µm. Data are expressed as mean $\pm$ SEM (n=3-5). *P < 0.05, ** P < 0.01 using Bonferroni's multiple comparison test.

MiR-124 NPs increase the number of migrating neuroblasts that reach the OB and the lesioned striatum leading to motor amelioration of the PD symptoms

Next, we evaluated the effect of miR-124 NPs in SVZ neurogenesis in a mouse model for PD. For that purpose, miR-124 NPs were unilaterally injected into the lateral ventricle, followed by 3 days of intraperitoneal injections with BrdU (every 12h) (Figure 7A). MiR-124 NPs were injected into the right lateral ventricle to facilitate the interaction with type B cells, which project one cilium each into the ventricle lumen [34]; alternatively, miR-124 NPs may interact with ependymal cells to induce a paracrine effect over SVZ stem/progenitor cells. Indeed, miR-Dye 547 loaded FITC-NPs delivered into the ventricular lumen were easily detected, lining the lateral ventricle of the SVZ, at 24 h after administration (Figure 7B). Then, to unveil the effect of our NP formulation in a pre-clinical mouse model for PD, mice were subjected to a double stereotaxic injection to

deliver 6-OHDA into the right striatum and the NPs into the right lateral ventricle (Figure 7A). This mouse model for PD (10 µg 6-OHDA in the striatum) was chosen based in the following parameters: reduced SVZ neurogenesis (about 40% reduction in $DCX^+/BrdU^+$ cells in the SVZ, Figure 7D), dopaminergic degeneration (about 50% dopaminergic death in the *SN*: 48.1 ± 6.1, n=10 mice), functional motor deficits (Figure 9D), and low mortality rates (in opposite to models such as involving injections in the *SN* or in the medial forebrain bundle). Mice were euthanized 4 weeks after stereotaxic surgeries and the number of neuroblasts (DCX^+), and proliferating neuroblasts ($DCX^+/BrdU^+$) were quantified in the SVZ (Figure 7) and in the GCL and GL of the OB (Figure 8). First, we found that miR-124 NPs were not able to alter the total number of DCX^+ (Figure 7C) and $DCX^+/BrdU^+$ cells (Figure 7D, E-H) in the SVZ of both healthy and 6-OHDA-treated mice as compared with the respective saline group. Nevertheless, the levels of proliferating neuroblasts ($DCX^+/BrdU^+$ cells) in 6-OHDA-treated mice were approximately 50% lower than in healthy mice. This may indicate a negative influence of striatal dopamine depletion over neuroblast proliferation and/or migration into lesioned regions (striatum) or into the OB. However, the total number of neuroblasts (DCX^+; Figure 7C) was not affected by dopamine depletion.

GCL and GL of the OB are the endpoint of SVZ-derived cells. In healthy animals, a significant increase in the number of DCX^+ (Figure 8A) and $DCX^+/BrdU^+$ (Figure 8B, C, D) cells was found in the GCL of mice treated with miR-124 NPs as compared with saline animals. It is plausible that these neuroblasts result not only from the division of stem/progenitor cells into neuronal progenitors ($DCX^+/BrdU^+$), but also from the neuronal commitment of cells that have not undergone mitosis, or from late dividing cells generated after the BrdU pulse (total DCX^+ cells). Then, we found that the number of DCX^+ and $DCX^+/BrdU^+$ cells was not significantly different between healthy saline and 6-OHDA saline mice (without miR-124 NP treatment). Interestingly, miR-124 NPs increased the number of DCX^+ (Figure 8A, C, D) and $DCX^+/BrdU^+$ (Figure 8B, E, F) cells found in the GCL of 6-OHDA-treated animals as compared with miR-124 NP-treated healthy mice. This may suggest that miR-124 NPs promote an overall increase in migrating neuroblasts in PD animals. Importantly, migrating neuroblasts reach the GCL fully differentiated into mature neurons

(NeuN[+]/BrdU[+]) (Supplementary Figure 1). Although we do not know the neuronal phenotype generated by DCX[+] neuroblasts found in the GCL, we do know that the GCL contains mostly SVZ-derived GABAergic interneurons [50,51].
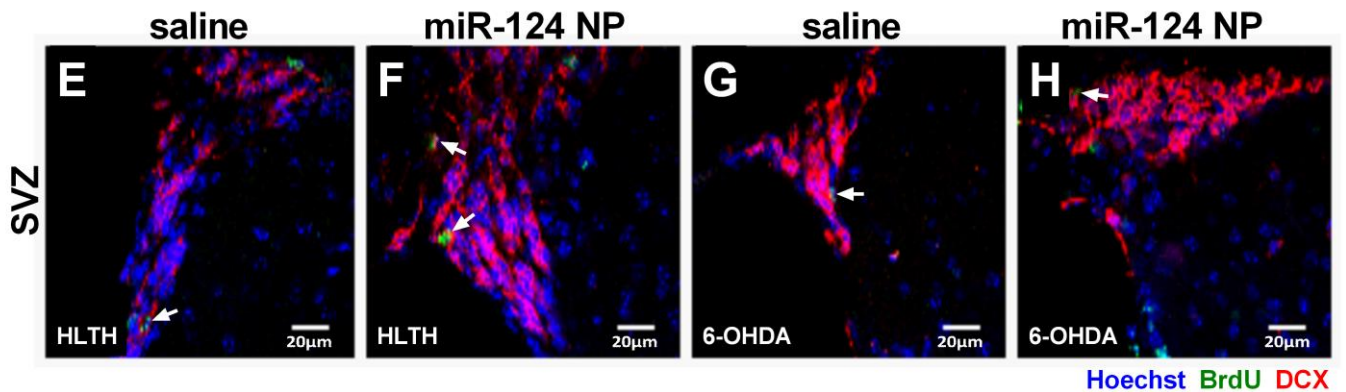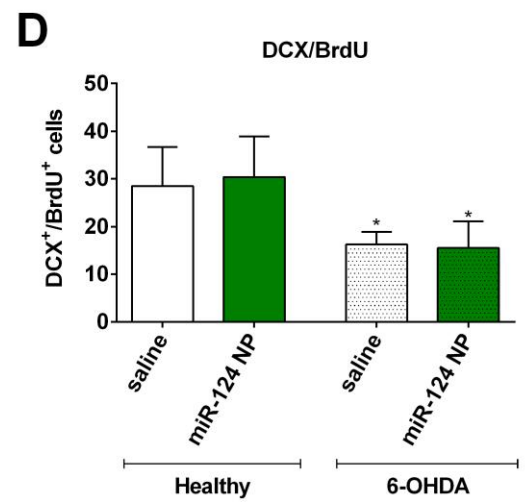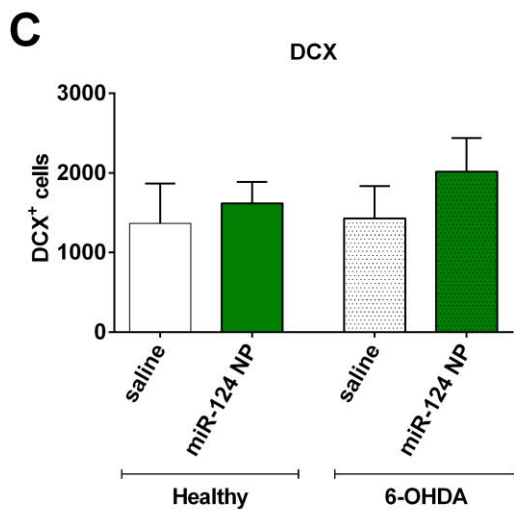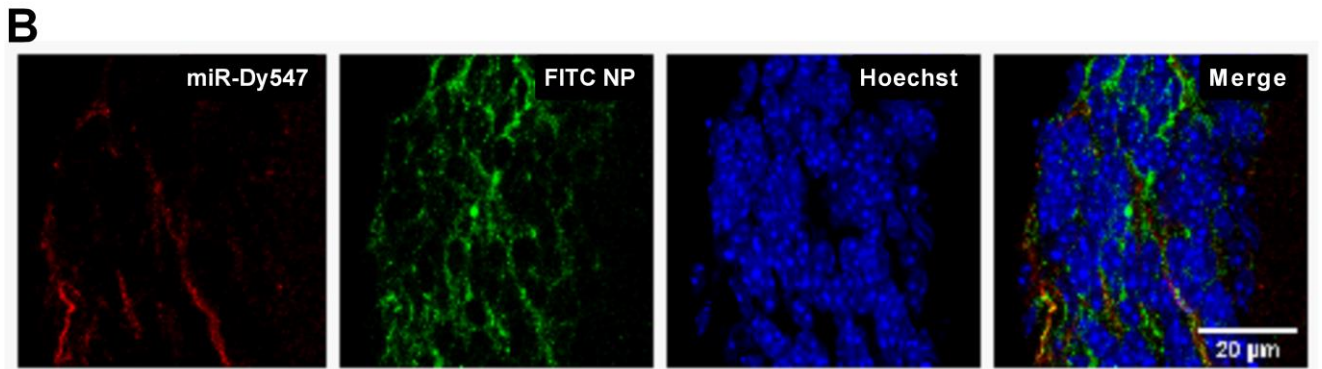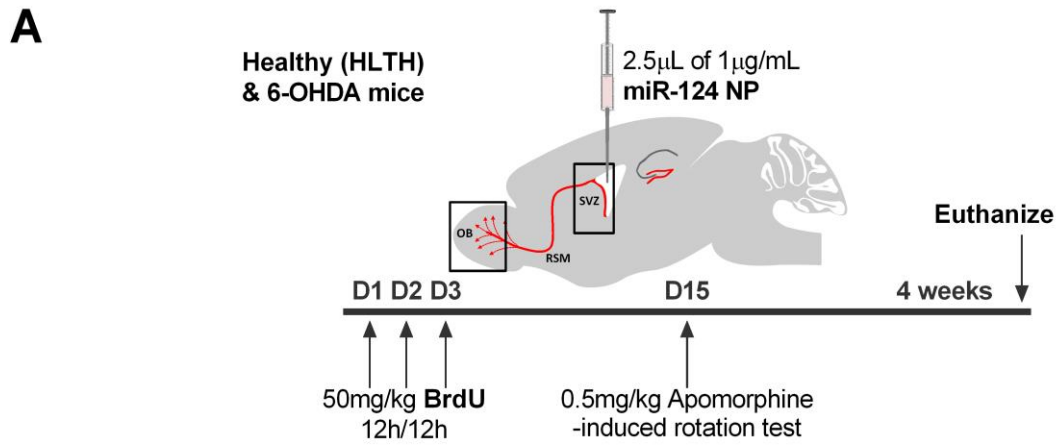
In physiological conditions neuroblasts originated in the SVZ migrate through the rostral migratory stream towards the OB. However, upon brain damage, neuroblasts can also migrate towards the lesion replacing damaged or dead neurons [34]. Accordingly, some proliferating neuroblasts (DCX[+]/BrdU[+]) (Supplementary Figure 2) as well as mature neurons (NeuN[+]/BrdU[+]) (Figure 9A, B, C) were found in the striatum of 6-OHDA-treated mice, demonstrating that DA depletion *per se* activated endogenous brain repair mechanisms. Importantly, miR-124 NPs further increased the number of mature neurons found in the lesioned striatum of 6-OHDA-treated mice (Figure 9A, B, C). As expected, the levels of NeuN[+]/BrdU^{+} cells in the striatum were almost inexistent in healthy mice. Our *in vivo* data suggest that miR-124 NPs reinforce the migration of SVZ-derived neurons towards the lesioned striatum of 6-OHDA treated mice, likely as an attempt to promote brain repair.

It is known that unilateral injections of 6-OHDA in mice and/or rats have the advantage, when compared with other PD mice models, of presenting side-biased motor impairments [52,53]. Apomorphine is a dopamine receptor agonist that at low doses causes contralateral turning by stimulating both supersensitive D1 and D2 receptors preferentially on the denervated side (contralateral side) [54]. Apomorphine-rotation test is used not only to characterize the extent of lesion but also to detect therapeutic effects. To unveil if our treatment has any impact into the amelioration of PD symptoms in the 6-OHDA-lesioned mice we performed a behavioral analysis based on the apomorphine-rotation test (Figure 9D). Two weeks after the stereotaxic injections, apomorphine was administrated subcutaneously and rotation to the contralateral or ipsilateral side registered for 45 min. As expected, healthy mice, both saline and miR-124 NP treated mice, exhibited a net rotation near zero, while 6-OHDA-lesioned saline mice presented a significant increase in the net contralateral rotations that was reversed at some extent in miR-124 NP treated mice (Figure 9D). Although any significant differences were found in the levels of dopaminergic neurons in the SN of 6-OHDA-lesioned mice (saline and miR-124 NPs, data not shown), the boost of

neurogenesis caused by our formulation seems to partly rescue the motor impairments of 6-OHDA-lesioned mice.

Previous reports showed that miR-124 overexpression promotes neurogenesis and decreases SVZ proliferation in physiological conditions. Moreover, it does not interfere with migration nor OB integration [13,14], but it endorses a preferential integration of new neurons into the GCL rather than the GL [14]. Accordingly, we showed that a single intracerebroventricular administration of miR-124 NPs is able to modulate SVZ neurogenesis, culminating in the enrichment of new neurons in the GCL of the OB. Then, we hypothesized that miR-124 NPs are also able to boost neurogenesis in a mouse model for PD. PD pathology can cause neurogenesis impairment despite the controversy on this matter (reviewed by Van den Bern et al, 2013 [55]). For example, injection of 6-OHDA in mice led to a reduction in SVZ proliferation [56,57], yet the levels of neuroblasts in SVZ and RMS were not affected and a higher survival of neurons in the OB was detected [57]. We also observed a reduction in SVZ proliferation caused by 6-OHDA that did not interfere with migration or OB integration. Even in pathological conditions, a single dose of miR-124 NPs was able to efficiently increase the number of migrating neuroblasts reaching the GCL to levels higher than the ones obtained when miR-124 NPs were administered in healthy animals. Importantly, miR-124 NPs potentiated the migration of SVZ-derived neurons towards the striatal damaged area. The above mentioned alterations culminated with the amelioration of the behavior of PD mice injected with miR-124 NPs. Although the levels of dopaminergic neurons in the SN of 6-OHDA challenged mice were similar between saline and miR-124 NP treated mice (data not shown), we anticipate that the higher levels of new neurons found in the striatum of 6-OHDA-treated miR-124 NP mice may contribute to the recovery outcome. Yet, future studies are needed to further disclose the involvement of other cells and/or mechanisms induced by miR-124 NPs responsible to induce motor recovery, such as neuroprotection [20,21] or reduction of neuroinflammation [58–60]. Taken together, our results suggest that miR-124 NPs are an attractive future therapeutic approach to potentiate the endogenous recovery of the injured brain, namely in PD.

A Healthy (HLTH) & 6-OHDA mice

2.5µL of 1µg/mL **miR-124 NP**

OB
SVZ
RSM

Euthanize

D1 D2 D3   D15   4 weeks

50mg/kg **BrdU**
12h/12h

0.5mg/kg Apomorphine
-induced rotation test

B
miR-Dy547 | FITC NP | Hoechst | Merge
20 µm

C DCX

DCX+ cells

saline | miR-124 NP | saline | miR-124 NP
Healthy | 6-OHDA

D DCX/BrdU

DCX+/BrdU+ cells

saline | miR-124 NP | saline | miR-124 NP
Healthy | 6-OHDA

saline | miR-124 NP | saline | miR-124 NP

SVZ

E HLTH | **F** HLTH | **G** 6-OHDA | **H** 6-OHDA
20µm | 20µm | 20µm | 20µm

Hoechst BrdU DCX

Figure 7. MiR-124 NPs do not affect the number of proliferating SVZ neuroblasts both in the healthy and in the 6-OHDA mouse model of PD. (A) Experimental design for the *in vivo* experiments consisting in an intracerebroventricular injection with miR-124 NPs or saline solution followed by the injection of 6-OHDA into the right striatum. Then, mice received BrdU injections (every 12 h) during the following 3-day upon surgery. After 4 weeks mice brains were collected for processing. (B) Representative photomicrographs of SVZ 24 h after injection, into the lumen of the lateral ventricle of mice, of 10 µg/mL of FITC-NPs (green) complexed with miR-Dy547 (red) and stained against the nuclear marker Hoechst (blue). (C, D) Bar graphs depict total (C) DCX$^+$ and (D) DCX$^+$/BrdU$^+$ cells counted in the SVZ. Data are expressed as mean ± SEM (n=3–5 mice) *P < 0.05 using Student's unpaired t-test as compared with saline healthy mice. (E-H) Representative confocal digital images of BrdU (green), DCX (red) and Hoechst (blue) staining observed in the SVZ of healthy (saline (D) or miR-124 NPs (E)) and 6-OHDA-injected mice (saline (F) or miR-124 NPs (G), respectively). Scale bar: 20 µm; white arrows indicate DCX$^+$/BrdU$^+$ cells.
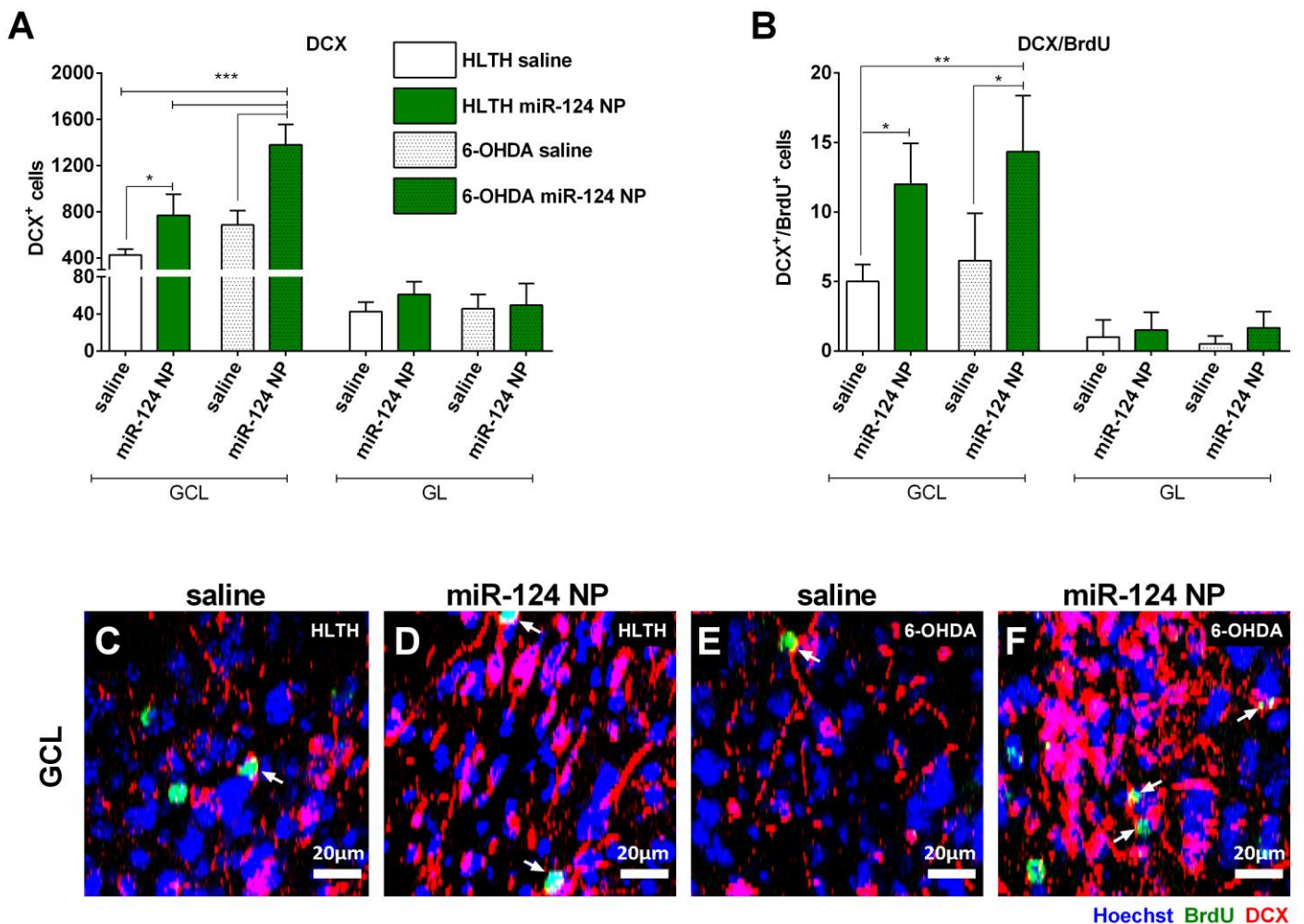
Figure 8. MiR-124 NPs induce migration of SVZ-derived neuroblasts towards the granule cell layer (GCL). (A, B) Bar graphs depict the effect of miR-124 NPs in the total number of (A) DCX$^+$ and (B) DCX$^+$/BrdU$^+$ cells in the granule cell layer (GCL) and glomerular layer (GL) of healthy or 6-OHDA-lesioned mice. Data are expressed as mean ± SEM (n=3–5 mice) *P <0.05, **P < 0.01, ***P < 0.001 using Bonferroni's multiple comparison test. (C-F) Representative confocal digital images of BrdU (green), Hoechst (blue) and DCX (red) staining observed in the GCL of healthy mice (saline (C) or miR-124 NPs (D)) or 6-OHDA-injected mice (saline (E) or miR-124 NPs (F)), respectively. Scale bar: 20µm; white arrows indicate DCX$^+$/BrdU$^+$ cells.
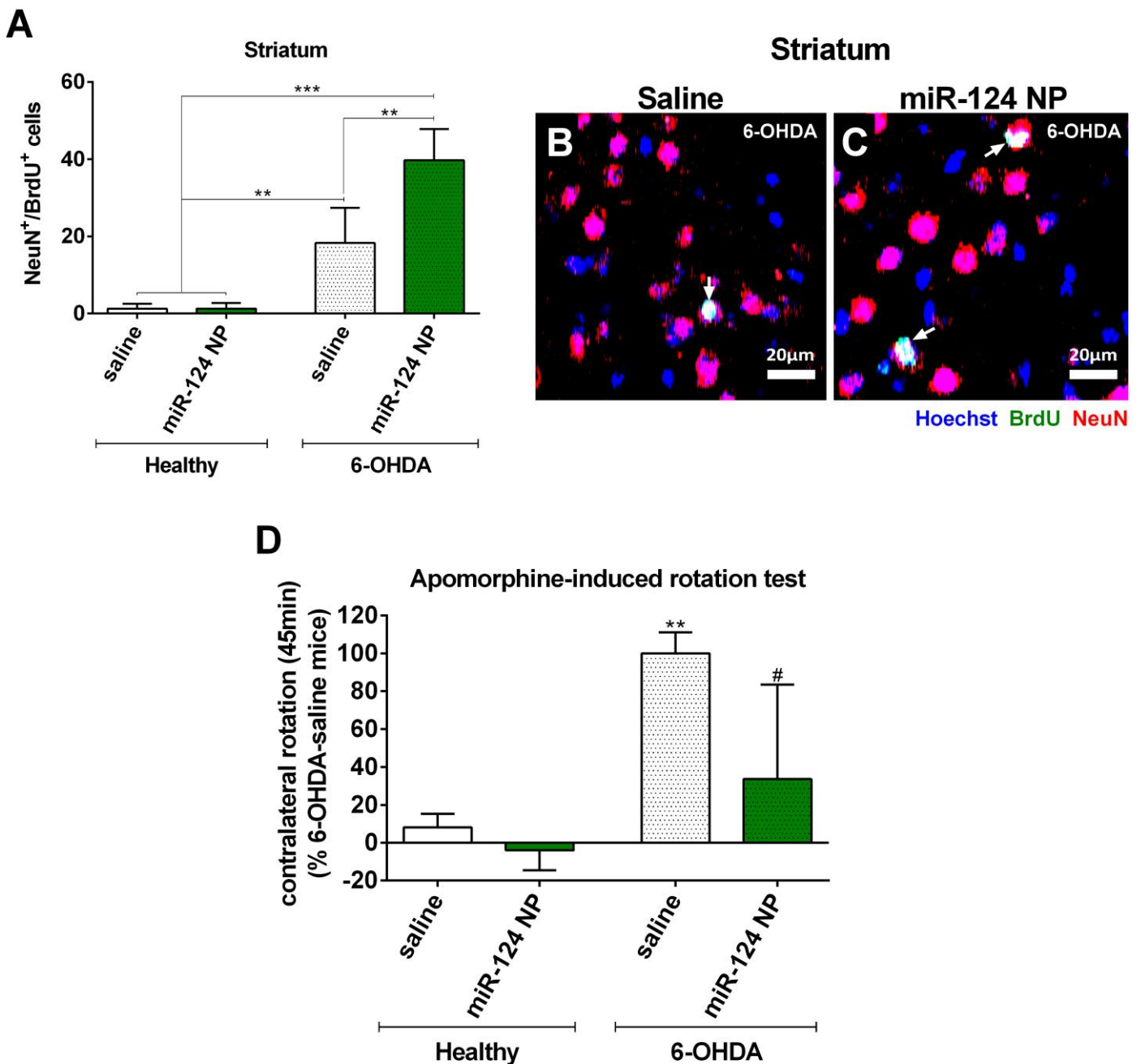
Figure 9. MiR-124 NPs induce integration of mature neurons into the lesioned striatum of 6-OHDA-treated mice and ameliorate the PD phenotype. (A) Bar graph depict the effect of miR-124 NPs on the total number of NeuN$^+$/BrdU$^+$ cells found in healthy or 6-OHDA-lesioned mice. (B, C) Representative confocal digital images of BrdU (green), Hoechst (blue) and NeuN (red) staining observed in the striatum of 6-OHDA-treated mice (saline (B) or miR-124 NPs (C)). Scale bar: 20 µm; white arrows highlight NeuN$^+$/BrdU$^+$ cells. (D) Bar graph illustrates the net rotation to the contralateral side of healthy or 6-OHDA-lesioned mice. Data are expressed as mean ± SEM (n=4-6 mice) #P<0.05, **P < 0.01, ***P < 0.001 using Bonferroni's multiple comparison test. (D) Results are set to 100%; # displays the difference between 6-OHDA-lesioned saline and miR-124 NPs mice.

Conclusions

To the best of our knowledge, this is the first report showing not only the ability of a NP formulation to modulate the endogenous neurogenic niche in PD but also its ability to ameliorate PD motor symptoms. Notably, we were able to demonstrate the pro-neurogenic potential of miR-124 NPs both in physiologic conditions and in a pre-clinical mouse model for PD. MiR-based therapies have been emerging in the last few years. Indeed, some clinical trials using miR-based therapies are being performed [61]. Nevertheless, one of the major concerns in the translation of miR-based therapies to the clinic is the efficient delivery of these molecules into cells. The physicochemical properties of miR (hydrophilic nature and negative charge) as well as their easy cleavage by nucleases make the transfection efficiency a challenge by itself [22,23]. We have developed a novel polymeric NP formulation which was efficiently internalized by NSCs, enhanced neurogenesis both in physiological and pathological conditions and can be traced by ^{19}F MRI technique [26]. The theranostic feature of our NPs makes it an attractive model to future clinical studies and an alternative to the NPs being currently used for MRI clinical application, such as superparamagnetic iron oxide NPs. Other important feature is the use of Food and Drug Administration (FDA)-approved materials in its composition [26] which can be engineered in terms of surface ligands making its delivery more specific and facilitating the translation to the clinic. Altogether, the NP formulation developed by us can overcome issues related with safety and traceability that other miR-delivery agents such as

viral vectors and liposomes cannot [22,23]. Most importantly, the formulation has already shown to be efficient in the delivery of miR into endothelial cells [26]. The biological effects of miR delivery previously described were higher than the ones obtained by commercial transfection reagents [26]. Herein, we proved that the uptake of miR-124 NPs by SVZ stem/progenitor cells resulted in the repression of Sox9 and Jagged1 proteins and the activation of SAPK/JNK pathway, promoting an increase in neurogenesis and axonogenesis. *In vivo*, a single administration of a small amount of miR-124 (0.5 pmol) delivered by our NP formulation increased the number of migrating SVZ-derived neuroblasts that reached the GCL of the OB, both in healthy and a PD mouse model. Importantly, mir-124 NPs also potentiated the migration of SVZ-derived neurons into the 6-OHDA lesioned striatum. The formulation promoted not only neurogenesis at the SVZ-OB axis but also the migration and maturation of new neurons into the lesioned striatum, indicating its value as a strategy to improve brain repair for PD. Moreover, our formulation also leads to motor amelioration of the PD symptoms found in 6-OHDA lesioned mice. As so, evidences of behavior improvement in pre-clinical models of PD can open new avenues in the development of novel therapeutic approaches. The systemic delivery of miR-124 NPs by intravenous or intraperitoneal injections should be considered in future studies to circumvent the need of an invasive stereotaxic surgery. To maximize the ability of NPs to cross the BBB, NPs should be coated with ligands or antibodies that are recognized by receptors/transporters or epitopes on brain endothelial cells [62,63]. In line with recent data showing beneficial effects induced by miR-124 on PD (neuroprotective agent) [20,21], Alzheimer's disease (alleviated cell death) [64], stroke (decreased infarct volume)[58,65], among others [3], our results provide clear evidences to support the use of miR-124 NPs as a new therapeutic approach to boost endogenous brain repair mechanisms in a setting of neurodegeneration.

References

[1]   F.H. Gage, Mammalian neural stem cells., Science. 287 (2000) 1433–8. doi:10.1126/science.287.5457.1433.

[2]   G.-L. Ming, H. Song, Adult neurogenesis in the mammalian brain: significant answers and significant questions., Neuron. 70 (2011) 687–702. doi:10.1016/j.neuron.2011.05.001.

[3]   Y. Sun, Z.-M. Luo, X.-M. Guo, D.-F. Su, X. Liu, An updated role of microRNA-124 in central nervous system disorders: a review, Front. Cell. Neurosci. 9 (2015) 1–8. doi:10.3389/fncel.2015.00193.

[4]   T. Kadota, T. Shingo, T. Yasuhara, N. Tajiri, A. Kondo, T. Morimoto, W.J. Yuan, F. Wang, T. Baba, K. Tokunaga, Y. Miyoshi, I. Date, Continuous intraventricular infusion of erythropoietin exerts neuroprotective/rescue effects upon Parkinson's disease model of rats with enhanced neurogenesis., Brain Res. 1254 (2009) 120–7. doi:10.1016/j.brainres.2008.11.094.

[5]   X. Jing, H. Miwa, T. Sawada, I. Nakanishi, T. Kondo, M. Miyajima, K. Sakaguchi, Ephrin-A1-mediated dopaminergic neurogenesis and angiogenesis in a rat model of Parkinson's disease., PLoS One. 7 (2012) e32019. doi:10.1371/journal.pone.0032019.

[6]   R. Faigle, H. Song, Signaling mechanisms regulating adult neural stem cells and neurogenesis., Biochim. Biophys. Acta. 1830 (2013) 2435–48. doi:10.1016/j.bbagen.2012.09.002.

[7]   T. Santos, R. Ferreira, J. Maia, F. Agasse, S. Xapelli, L. Cortes, J. Bragança, J.O.

Malva, L. Ferreira, L. Bernardino, Polymeric nanoparticles to control the differentiation of neural stem cells in the subventricular zone of the brain., ACS Nano. 6 (2012) 10463–74. doi:10.1021/nn304541h.

[8]   M.F. Eiriz, J. Valero, J.O. Malva, L. Bernardino, New insights into the role of histamine in subventricular zone-olfactory bulb neurogenesis, Front. Neurosci. 8 (2014) 1–7. doi:10.3389/fnins.2014.00142.

[9]   L. Zeng, X. He, Y. Wang, Y. Tang, C. Zheng, H. Cai, J. Liu, Y. Fu, G.-Y. Yang, MicroRNA-210 overexpression induces angiogenesis and neurogenesis in the normal adult mouse brain., Gene Ther. 21 (2014) 37–43. doi:10.1038/gt.2013.55.

[10]   L.P. Lim, N.C. Lau, P. Garrett-Engele, A. Grimson, J.M. Schelter, J. Castle, D.P. Bartel, P.S. Linsley, J.M. Johnson, Microarray analysis shows that some microRNAs downregulate large numbers of target mRNAs., Nature. 433 (2005) 769–773. doi:10.1038/nature03315.

[11]   D.P. Bartel, MicroRNAs: Genomics, Biogenesis, Mechanism, and Function, Cell. 116 (2004) 281–297. doi:10.1016/S0092-8674(04)00045-5.

[12]   M. Lagos-Quintana, R. Rauhut, A. Yalcin, J. Meyer, W. Lendeckel, T. Tuschl, Identification of Tissue-Specific MicroRNAs from Mouse, Curr. Biol. 12 (2002) 735–739. doi:10.1016/S0960-9822(02)00809-6.

[13]   L.-C. Cheng, E. Pastrana, M. Tavazoie, F. Doetsch, miR-124 regulates adult neurogenesis in the subventricular zone stem cell niche., Nat. Neurosci. 12 (2009) 399–408. doi:10.1038/nn.2294.

[14]   M. Akerblom, R. Sachdeva, I. Barde, S. Verp, B. Gentner, D. Trono, J. Jakobsson, MicroRNA-124 Is a Subventricular Zone Neuronal Fate Determinant, J. Neurosci. 32 (2012) 8879–8889. doi:10.1523/JNEUROSCI.0558-12.2012.

[15]   J. Yu, K. Chung, M. Deo, R.C. Thompson, D.L. Turner, MicroRNA miR-124 regulates neurite outgrowth during neuronal differentiation, Exp. Cell Res. 314 (2008) 2618–2633. doi:10.1016/j.yexcr.2008.06.002.

[16]   J. Visvanathan, S. Lee, B. Lee, J.W. Lee, S.-K. Lee, The microRNA miR-124 antagonizes the anti-neural REST/SCP1 pathway during embryonic CNS

development., Genes Dev. 21 (2007) 744–9. doi:10.1101/gad.1519107.

[17] A.S. Yoo, A.X. Sun, L. Li, A. Shcheglovitov, T. Portmann, Y. Li, C. Lee-Messer, R.E. Dolmetsch, R.W. Tsien, G.R. Crabtree, MicroRNA-mediated conversion of human fibroblasts to neurons., Nature. 476 (2011) 228–31. doi:10.1038/nature10323.

[18] Y. Xue, K. Ouyang, J. Huang, Y. Zhou, H. Ouyang, H. Li, G. Wang, Q. Wu, C. Wei, Y. Bi, L. Jiang, Z. Cai, H. Sun, K. Zhang, Y. Zhang, J. Chen, X.-D. Fu, Direct conversion of fibroblasts to neurons by reprogramming PTB-regulated microRNA circuits., Cell. 152 (2013) 82–96. doi:10.1016/j.cell.2012.11.045.

[19] K.-C. Sonntag, MicroRNAs and deregulated gene expression networks in neurodegeneration., Brain Res. 1338 (2010) 48–57. doi:10.1016/j.brainres.2010.03.106.

[20] N. Kanagaraj, H. Beiping, S.T. Dheen, S.S.W. Tay, Downregulation of miR-124 in MPTP-treated mouse model of Parkinson's disease and MPP iodide-treated MN9D cells modulates the expression of the calpain/cdk5 pathway proteins., Neuroscience. 272 (2014) 167–79. doi:10.1016/j.neuroscience.2014.04.039.

[21] H. Wang, Y. Ye, Z. Zhu, L. Mo, C. Lin, Q. Wang, H. Wang, X. Gong, X. He, G. Lu, F. Lu, S. Zhang, MiR-124 Regulates Apoptosis and Autophagy Process in MPTP Model of Parkinson's Disease by Targeting to Bim, Brain Pathol. (2015). doi:10.1111/bpa.12267.

[22] Y. Chen, H. Zhao, Z. Tan, C. Zhang, X. Fu, Bottleneck limitations for microRNA-based therapeutics from bench to the bedside., Pharmazie. 70 (2015) 147–54. doi:91/ph.2015.4774.

[23] D. Guzman-Villanueva, I.M. El-Sherbiny, D. Herrera-Ruiz, A. V. Vlassov, H.D.C. Smyth, Formulation approaches to short interfering RNA and MicroRNA: Challenges and implications, J. Pharm. Sci. 101 (2012) 4046–4066. doi:10.1002/jps.23300.

[24] J. Maia, T. Santos, S. Aday, F. Agasse, L. Cortes, J.O. Malva, L. Bernardino, L. Ferreira, Controlling the neuronal differentiation of stem cells by the intracellular delivery of retinoic acid-loaded nanoparticles., ACS Nano. 5 (2011) 97–106.

doi:10.1021/nn101724r.

[25] L. Bernardino, M.F. Eiriz, T. Santos, S. Xapelli, S. Grade, A.I. Rosa, L. Cortes, R. Ferreira, J. Bragança, F. Agasse, L. Ferreira, J.O. Malva, Histamine stimulates neurogenesis in the rodent subventricular zone., Stem Cells. 30 (2012) 773–84. doi:10.1002/stem.1042.

[26] R.S.M. Gomes, R.P. Das Neves, L. Cochlin, A. Lima, R. Carvalho, P. Korpisalo, G. Dragneva, M. Turunen, T. Liimatainen, K. Clarke, S. Ylä-Herttuala, C. Carr, L. Ferreira, Efficient Pro-survival/angiogenic miRNA Delivery by an MRI-Detectable Nanomaterial., ACS Nano. 7 (2013) 3362–72. doi:10.1021/nn400171w.

[27] F. Agasse, L. Bernardino, B. Silva, R. Ferreira, S. Grade, J.O. Malva, Response to histamine allows the functional identification of neuronal progenitors, neurons, astrocytes, and immature cells in subventricular zone cell cultures., Rejuvenation Res. 11 (2008) 187–200. doi:10.1089/rej.2007.0600.

[28] A.I. Rosa, J. Gonçalves, L. Cortes, L. Bernardino, J.O. Malva, F. Agasse, The angiogenic factor angiopoietin-1 is a proneurogenic peptide on subventricular zone stem/progenitor cells., J. Neurosci. 30 (2010) 4573–84. doi:10.1523/JNEUROSCI.5597-09.2010.

[29] L. Bernardino, F. Agasse, B. Silva, R. Ferreira, S. Grade, J.O. Malva, Tumor necrosis factor-alpha modulates survival, proliferation, and neuronal differentiation in neonatal subventricular zone cell cultures., Stem Cells. 26 (2008) 2361–71. doi:10.1634/stemcells.2007-0914.

[30] F. Agasse, L. Bernardino, H. Kristiansen, S.H. Christiansen, R. Ferreira, B. Silva, S. Grade, D.P.D. Woldbye, J.O. Malva, Neuropeptide Y promotes neurogenesis in murine subventricular zone., Stem Cells. 26 (2008) 1636–45. doi:10.1634/stemcells.2008-0056.

[31] A. Virgone-Carlotta, J. Uhlrich, M.N. Akram, D. Ressnikoff, F. Chrétien, C. Domenget, R. Gherardi, G. Despars, P. Jurdic, J. Honnorat, S. Nataf, M. Touret, Mapping and kinetics of microglia/neuron cell-to-cell contacts in the 6-OHDA murine model of Parkinson's disease, Glia. 61 (2013) 1645–1658.

doi:10.1002/glia.22546.

[32] J.M. Wojtowicz, N. Kee, BrdU assay for neurogenesis in rodents, Nat. Protoc. 1 (2006) 1399–1405. doi:10.1038/nprot.2006.224.

[33] J. Ruiz-Cabello, B.P. Barnett, P.A. Bottomley, J.W.M. Bulte, Fluorine (19F) MRS and MRI in biomedicine., NMR Biomed. 24 (2011) 114–29. doi:10.1002/nbm.1570.

[34] T. Santos, J. Maia, F. Agasse, S. Xapelli, L. Ferreira, L. Bernardino, Nanomedicine boosts neurogenesis: new strategies for brain repair, Integr Biol. 4 (2012) 973–981. doi:10.1039/c2ib20129a.

[35] E. Fröhlich, The role of surface charge in cellular uptake and cytotoxicity of medical nanoparticles., Int. J. Nanomedicine. 7 (2012) 5577–91. doi:10.2147/IJN.S36111.

[36] B. Menn, J.M. Garcia-Verdugo, C. Yaschine, O. Gonzalez-Perez, D. Rowitch, A. Alvarez-Buylla, Origin of Oligodendrocytes in the Subventricular Zone of the Adult Brain, J. Neurosci. 26 (2006) 7907–7918. doi:10.1523/JNEUROSCI.1299-06.2006.

[37] W.H. Neo, K. Yap, S.H. Lee, L.S. Looi, P. Khandelia, S.X. Neo, E. V. Makeyev, I.H. Su, MicroRNA miR-124 controls the choice between neuronal and astrocyte differentiation by fine-tuning Ezh2 expression, J. Biol. Chem. 289 (2014) 20788–20801. doi:10.1074/jbc.M113.525493.

[38] M. Akerblom, J. Jakobsson, MicroRNAs as Neuronal Fate Determinants., Neuroscientist. 20 (2013) 235–242. doi:10.1177/1073858413497265.

[39] C.C. Stolt, P. Lommes, E. Sock, M.-C. Chaboissier, A. Schedl, M. Wegner, The Sox9 transcription factor determines glial fate choice in the developing spinal cord., Genes Dev. 17 (2003) 1677–89. doi:10.1101/gad.259003.

[40] Y. Nyfeler, R.D. Kirch, N. Mantei, D.P. Leone, F. Radtke, U. Suter, V. Taylor, Jagged1 signals in the postnatal subventricular zone are required for neural stem cell self-renewal., EMBO J. 24 (2005) 3504–15. doi:10.1038/sj.emboj.7600816.

[41] A. a Oliva, C.M. Atkins, L. Copenagle, G. a Banker, Activated c-Jun N-terminal

kinase is required for axon formation., J. Neurosci. 26 (2006) 9462–9470. doi:10.1523/JNEUROSCI.2625-06.2006.

[42] C. Weston, The JNK signal transduction pathway, Curr. Opin. Genet. Dev. 12 (2002) 14–21. doi:10.1016/S0959-437X(01)00258-1.

[43] E.E. Varfolomeev, A. Ashkenazi, Tumor Necrosis Factor, Cell. 116 (2004) 491–497. doi:10.1016/S0092-8674(04)00166-7.

[44] A.M. Bode, Z. Dong, The functional contrariety of JNK., Mol. Carcinog. 46 (2007) 591–8. doi:10.1002/mc.20348.

[45] P. Xu, K. Yoshioka, D. Yoshimura, Y. Tominaga, T. Nishioka, M. Ito, Y. Nakabeppu, In vitro development of mouse embryonic stem cells lacking JNK/stress-activated protein kinase-associated protein 1 (JSAP1) scaffold protein revealed its requirement during early embryonic neurogenesis., J. Biol. Chem. 278 (2003) 48422–33. doi:10.1074/jbc.M307888200.

[46] C.R. Amura, L. Marek, R.A. Winn, L.E. Heasley, Inhibited neurogenesis in JNK1-deficient embryonic stem cells., Mol. Cell. Biol. 25 (2005) 10791–802. doi:10.1128/MCB.25.24.10791-10802.2005.

[47] A.A. Oliva, C.M. Atkins, L. Copenagle, G.A. Banker, Activated c-Jun N-terminal kinase is required for axon formation., J. Neurosci. 26 (2006) 9462–70. doi:10.1523/JNEUROSCI.2625-06.2006.

[48] H. Yoshida, C.J. Hastie, H. McLauchlan, P. Cohen, M. Goedert, Phosphorylation of microtubule-associated protein tau by isoforms of c-Jun N-terminal kinase (JNK)., J. Neurochem. 90 (2004) 352–8. doi:10.1111/j.1471-4159.2004.02479.x.

[49] X. Gu, S. Meng, S. Liu, C. Jia, Y. Fang, S. Li, C. Fu, Q. Song, L. Lin, X. Wang, MiR-124 Represses ROCK1 Expression to Promote Neurite Elongation Through Activation of the PI3K/Akt Signal Pathway, J. Mol. Neurosci. 52 (2014) 156–165. doi:10.1007/s12031-013-0190-6.

[50] A. Bédard, A. Parent, Evidence of newly generated neurons in the human olfactory bulb, Dev. Brain Res. 151 (2004) 159–168. doi:10.1016/j.devbrainres.2004.03.021.

[51] S. De Marchis, S. Temoney, F. Erdelyi, S. Bovetti, P. Bovolin, G. Szabo, A.C. Puche, GABAergic phenotypic differentiation of a subpopulation of subventricular derived migrating progenitors, Eur. J. Neurosci. 20 (2004) 1307–1317. doi:10.1111/j.1460-9568.2004.03584.x.

[52] U. Ungerstedt, G.W. Arbuthnott, Quantitative recording of rotational behavior in rats after 6-hydroxy-dopamine lesions of the nigrostriatal dopamine system, Brain Res. 24 (1970) 485–493. doi:10.1016/0006-8993(70)90187-3.

[53] R. Iancu, P. Mohapel, P. Brundin, G. Paul, Behavioral characterization of a unilateral 6-OHDA-lesion model of Parkinson's disease in mice., Behav. Brain Res. 162 (2005) 1–10. doi:10.1016/j.bbr.2005.02.023.

[54] M.J. Millan, L. Maiofiss, D. Cussac, V. Audinot, J.-A. Boutin, A. Newman-Tancredi, Differential actions of antiparkinson agents at multiple classes of monoaminergic receptor. I. A multivariate analysis of the binding profiles of 14 drugs at 21 native and cloned human receptor subtypes., J. Pharmacol. Exp. Ther. 303 (2002) 791–804. doi:10.1124/jpet.102.039867.

[55] S. a van den Berge, M.E. van Strien, E.M. Hol, Resident adult neural stem cells in Parkinson's disease--the brain's own repair system?, Eur. J. Pharmacol. 719 (2013) 117–27. doi:10.1016/j.ejphar.2013.04.058.

[56] S. a Baker, K.A. Baker, T. Hagg, Dopaminergic nigrostriatal projections regulate neural precursor proliferation in the adult mouse subventricular zone., Eur. J. Neurosci. 20 (2004) 575–9. doi:10.1111/j.1460-9568.2004.03486.x.

[57] Y. Sui, M.K. Horne, D. Stanić, Reduced proliferation in the adult mouse subventricular zone increases survival of olfactory bulb interneurons., PLoS One. 7 (2012) e31549. doi:10.1371/journal.pone.0031549.

[58] T.R. Doeppner, M. Doehring, E. Bretschneider, A. Zechariah, B. Kaltwasser, B. Müller, J.C. Koch, M. Bähr, D.M. Hermann, U. Michel, MicroRNA-124 protects against focal cerebral ischemia via mechanisms involving Usp14-dependent REST degradation., Acta Neuropathol. 126 (2013) 251–65. doi:10.1007/s00401-013-1142-5.

[59] Y. Sun, Q. Li, H. Gui, D.-P. Xu, Y.-L. Yang, D.-F. Su, X. Liu, MicroRNA-124

mediates the cholinergic anti-inflammatory action through inhibiting the production of pro-inflammatory cytokines, Cell Res. 23 (2013) 1270–1283. doi:10.1038/cr.2013.116.

[60] R.W. Freilich, M.E. Woodbury, T. Ikezu, Integrated expression profiles of mRNA and miRNA in polarized primary murine microglia., PLoS One. 8 (2013) e79416. doi:10.1371/journal.pone.0079416.

[61] F. Wahid, T. Khan, Y.Y. Kim, MicroRNA and diseases: Therapeutic potential as new generation of drugs, Biochimie. 104 (2014) 12–26. doi:10.1016/j.biochi.2014.05.004.

[62] D.T. Wiley, P. Webster, A. Gale, M.E. Davis, Transcytosis and brain uptake of transferrin-containing nanoparticles by tuning avidity to transferrin receptor., Proc. Natl. Acad. Sci. U. S. A. 110 (2013) 8662–7. doi:10.1073/pnas.1307152110.

[63] C. Saraiva, C. Praça, R. Ferreira, T. Santos, L. Ferreira, L. Bernardino, Nanoparticle-mediated brain drug delivery: Overcoming blood-brain barrier to treat neurodegenerative diseases, J. Control. Release. (2016). doi:10.1016/j.jconrel.2016.05.044.

[64] M. Fang, J. Wang, X. Zhang, Y. Geng, Z. Hu, J.A. Rudd, S. Ling, W. Chen, S. Han, The miR-124 regulates the expression of BACE1/β-secretase correlated with cell death in Alzheimer's disease., Toxicol. Lett. 209 (2012) 94–105. doi:10.1016/j.toxlet.2011.11.032.

[65] Y. Sun, H. Gui, Q. Li, Z.-M. Luo, M.-J. Zheng, J.-L. Duan, X. Liu, MicroRNA-124 protects neurons against apoptosis in cerebral ischemic stroke., CNS Neurosci. Ther. 19 (2013) 813–9. doi:10.1111/cns.12142.